

Replacement of the Axial Histidine Ligand with Imidazole in Cytochrome *c* Peroxidase. 1. Effects on Structure<sup>†,‡</sup>Judy Hirst,<sup>§,||</sup> Sheri K. Wilcox,<sup>§,-</sup> Pamela A. Williams,<sup>#</sup> John Blankenship, Duncan E. McRee, and David B. Goodin\**Department of Molecular Biology, MB8, The Scripps Research Institute, 10550 North Torrey Pines Road, La Jolla, California 92037**Received September 5, 2000; Revised Manuscript Received November 20, 2000*

**ABSTRACT:** Replacement of the axial histidine ligand with exogenous imidazole has been accomplished in a number of heme protein mutants, where it often serves to complement the functional properties of the protein. In this paper, we describe the effects of pH and buffer ion on the crystal structure of the H175G mutant of cytochrome *c* peroxidase, in which the histidine tether between the heme and the protein backbone is replaced by bound imidazole. The structures show that imidazole can occupy the proximal H175G cavity under a number of experimental conditions, but that the details of the interaction with the protein and the coordination to the heme are markedly dependent on conditions. Replacement of the tethered histidine ligand with imidazole permits the heme to shift slightly in its pocket, allowing it to adopt either a planar or distally domed conformation. H175G crystallized from both high phosphate and imidazole concentrations exists as a novel, 5-coordinate phosphate bound state, in which the proximal imidazole is dissociated and the distal phosphate is coordinated to the iron. To accommodate this bound phosphate, the side chains of His-52 and Asn-82 alter their positions and a significant conformational change in the surrounding protein backbone occurs. In the absence of phosphate, imidazole binds to the proximal H175G cavity in a pH-dependent fashion. At pH 7, imidazole is directly coordinated to the heme ( $d_{\text{Fe-Im}} = 2.0 \text{ \AA}$ ) with a nearby distal water ( $d_{\text{Fe-HOH}} = 2.4 \text{ \AA}$ ). This is similar to the structure of WT CCP except that the iron lies closer in the heme plane, and the hydrogen bond between imidazole and Asp-235 ( $d_{\text{Im-Asp}} = 3.1 \text{ \AA}$ ) is longer than for WT CCP ( $d_{\text{His-Asp}} = 2.9 \text{ \AA}$ ). As the pH is dropped to 5, imidazole dissociates from the heme ( $d_{\text{Fe-Im}} = 2.9 \text{ \AA}$ ), but remains in the proximal cavity where it is strongly hydrogen bonded to Asp-235 ( $d_{\text{Im-Asp}} = 2.8 \text{ \AA}$ ). In addition, the heme is significantly domed toward the distal pocket where it may coordinate a water molecule. Finally, the structure of H175G/Im, pH 6, at low temperature (100 K) is very similar to that at room temperature, except that the water above the distal heme face is not present. This study concludes that steric restrictions imposed by the covalently tethered histidine restrain the heme and its ligand coordination from distortions that would arise in the absence of the restricted tether. Coupled with the functional and spectroscopic properties described in the following paper in this issue, these structures help to illustrate how the delicate and critical interactions between protein, ligand, and metal modulate the function of heme enzymes.

Metal ligand coordination plays a well recognized role in defining and modulating the properties of heme enzymes. Much of this understanding has come from systematic variation of model complexes (1–6), comparison of related

protein structures (7–9), and site-directed mutagenesis (10–13). Often however, mutagenesis can be a blunt tool because it is difficult to make enough subtle changes in a ligand identity or its interactions with the protein environment to produce meaningful relationships. The incorporation of unnatural amino acids has provided a promising solution to this problem (14), but in this case it can be difficult to obtain large enough quantities of the modified proteins for study. Chemical rescue (15) or cavity complementation (16) has provided an alternative method for replacing a targeted structural element by related but unnatural chemical entities. For several metalloproteins, it has been possible to replace metal ligand side chains with cavity forming mutants that allow binding by analogous exogenous ligands (12, 17–24). Subtle variations in ligand binding can then provide detailed information about the role of metal ligands, provided that the functional and spectroscopic properties are combined with detailed structural characterization.

<sup>†</sup> This work was supported in part by grants GM41049 and GM48495 from the National Institutes of Health to D.B.G. and D.E.M., and by a Wellcome Trust Prize International Research Fellowship to J.H.

<sup>‡</sup> The crystallographic coordinates for the structures presented in this work have been deposited with the Protein Data Bank, Research Collaboratory for Structural Bioinformatics (RCSB), (<http://www.rcsb.org>) entries 1DSE, 1DS4, 1DSG, 1DSO, and 1DSP.

\* To whom correspondence should be addressed. Phone: (858) 784-9892. Fax: (858) 784-2857. E-mail: [dbg@scripps.edu](mailto:dbg@scripps.edu).

<sup>§</sup> These authors contributed equally to this work.

<sup>||</sup> Current address: Medical Research Council, Dunn Human Nutrition Unit, Hills Rd., Cambridge, CB2 2XY, U.K.

<sup>-</sup> Current address: Pharmacia Corporation, Department of Protein Science, 301 Henrietta St., Kalamazoo, MI 49001.

<sup>#</sup> Current address: Laboratory of Molecular Biophysics, Rex Richards Building, University of Oxford, South Parks Road, Oxford, OX1 3QU, U.K.

Axial ligand replacement by exogenous imidazoles has been shown to restore native protein function in several heme proteins. Addition of imidazole (Im)<sup>1</sup> to histidine cavity mutants of both myoglobin (20) and heme oxygenase (22) resulted in properties similar to those of the native protein, indicating that exogenous imidazole is able to functionally replace the histidine side-chain. In studies of the H175G mutant of cytochrome *c* peroxidase (CCP), low-resolution crystal structures have demonstrated a structurally defined cavity capable of binding imidazole to give an active site that is similar to that of native enzyme (21). However, binding of the surrogate imidazole ligand to the H175G cavity did not restore the enzymatic activity. This result has proven difficult to reconcile with other data that have shown clearly that the axial His-175 can be replaced with Glu and Gln to give functional proteins (10, 25–27). This intriguing difference in properties, in which His can be replaced by a carboxylate or an amide with retention of activity, but not with imidazole has not previously been understood (12). Unlike other heme proteins, peroxidases impose unusual properties on the axial His ligand. In CCP, Asp-235 is strongly hydrogen bonded to both His-175 and Trp-191 (28). The resulting imidazolite character of His-175 is thought to promote peroxy bond cleavage during reaction with H<sub>2</sub>O<sub>2</sub> and to stabilize the resulting oxidized ferryl heme center, while the interactions with Trp-191 may effect the coupling and stability of the Trp-191 radical of the oxidized compound I state (29). The previous low-resolution structures of H175G were unable to provide detailed observations of the interactions between the Im ligand and this hydrogen bonding network (21). Thus the question of whether an exogenous imidazole is capable of participating effectively as part of this catalytic triad remained unresolved by previous studies. A second important question concerns the role of the Fe-His-Asp-Trp linkage in the electronic coupling between the heme and the Trp-191 free radical site and how changes in this network affect electron transfer from cytochrome *c* (cyt *c*), through Trp-191 to the heme (30–32). Finally, His-175 provides the only covalent linkage between the heme cofactor and the protein backbone, and there may be direct structural consequences from the loss of this protein tether. Clearly, the functional and structural deficiencies of the H175G/Im complex compared with the native enzyme arise from subtle and delicate alterations in the interactions of Im with the protein that have not yet been fully characterized.

Our investigation of the effects of replacing His-175 with exogenous imidazole is presented in two parts. In this first paper a number of crystal structures are reported for complexes of H175G with imidazole and phosphate. In our descriptions of these states, we use the nomenclature H175G/*X*<sub>c/d</sub>/*Y*<sub>c/d</sub> to represent the state in which ligand *X* occupies the proximal heme cavity and ligand *Y* occupies the distal heme cavity, and they are either coordinated (c) or dissociated (d) from the heme iron. A more simplified notation H175G/*X*

refers to the protein in the presence of ligand *X* where the occupation and coordination are unspecified. Results of these analyses show that removing the tether between protein backbone and axial ligand produces distinct changes in the active-site structure which are dependent on pH, counterion, and temperature. The functional and spectroscopic manifestations of this behavior are considered in detail in the following paper in this issue.

## EXPERIMENTAL METHODS

*Protein Expression and Purification and Crystal Growth.* Expression of CCP(MKT) and the H175G mutant from *E. coli* was carried out as described previously (19). Protein purification was also as described previously except for phosphate free preparations. In this case, following a first dialysis and batch crystallization against distilled water, the crystals were redissolved into 1 M MES buffer, pH 6, before being recrystallized for a second time. Single crystals for X-ray data collection were grown under several conditions for this study. It was not possible to grow crystals of H175G in the presence of phosphate by vapor diffusion against 2-methyl-2,4-pentanediol (MPD). Thus, crystals of H175G in the presence of Im and phosphate were grown at 4 C by microdialysis of a solution containing 0.4 mM protein, 500 mM potassium phosphate, pH 6, 10 mM imidazole, against a large volume of 50 mM potassium phosphate, pH 6, 10 mM imidazole. Crystals were soaked briefly in a cryoprotectant, 35% ethylene glycol or sucrose, 65% dialysate, before being mounted on a nylon loop and flash-freezing in a jet of nitrogen at 100 K for data collection. Crystals were also grown for H175G/Im at pH 5, 6, and 7 and low phosphate concentrations for room temperature data collection. These crystals were grown by micro-dialysis of a starting solution of 0.4 mM protein, 75 mM phosphate buffer, pH 6, 10 mM imidazole, against approximately 100 vol of 50 mM MES, 10 mM imidazole, at pH values of 5.2, 6.0, or 7.0. Finally, crystals of H175G/Im were grown in the absence of phosphate for cryogenic data collection (100 K) by vapor diffusion at 18 C from sitting drops of phosphate-free CCP, 8.5% MPD, 200 mM MES, pH 6.0, and 8.5 mM imidazole against a reservoir of 25% MPD. Crystals were briefly immersed in 25% MPD, 10 mM imidazole pH 6, as a cryoprotectant before mounting and freezing as described above.

*X-ray Crystallographic Data Collection and Analysis.* Several conditions of X-ray diffraction data collection were necessary for H175G/Im crystals. It was possible to collect low-temperature data (100 K) on H175G/Im/phosphate crystals using CuK $\alpha$  radiation from the rotating anode of a Siemens SRA X-ray generator. However, room-temperature crystals were very sensitive to radiation exposure and were found to diffract for less than an hour after initial exposure, regardless of the actual length of exposure. Thus, data for H175G/Im pH 5, 6, and 7 were collected at 8 on Beamline 7-1 at the Stanford Synchrotron Radiation Laboratory (SSRL) (Department Energy, Office of Basic Energy Sciences) using 2 s exposures. A low temperature (100 K) data set for H175G/Im, pH 6, in the absence of phosphate was also collected on SSRL Beamline 7-1.

Each data set was collected using a Mar Research (Hamburg, Germany) image plate with 1° oscillation and a crystal to plate distance of 120–200 mm as appropriate. Data

<sup>1</sup> Abbreviations: CCP(MKT), cytochrome *c* peroxidase produced by expression in *Escherichia coli* containing Met-Lys-Thr at the N-terminus, Ile at position 53, and Gly at position 152; CCP, cytochrome *c* peroxidase; cyt *c*, cytochrome *c*; H175G, mutant in which His-175 is replaced by Gly; H175G/*X*<sub>c/d</sub>/*Y*<sub>c/d</sub>, state in which ligand *X* occupies the proximal heme cavity, ligand *Y* occupies the distal heme cavity, and these are either coordinated (c) to or dissociated (d) from the heme iron; Im, imidazole; MPD, 2-methyl-2,4-pentanediol; SSRL, Stanford Synchrotron Radiation Laboratory; WT, wild-type CCP.

Table 1: Statistics for Crystallographic Data Collection and Refinement

	H175G/Im/phosphate	H175G/Im 100 K	H175G/Im pH 5	H175G/Im pH 6	H175G/Im pH 7
space group	$P2_12_12_1$	$P2_12_12_1$	$P2_12_12_1$	$P2_12_12_1$	$P2_12_12_1$
unit cell: $a$	107.26	106.90	107.90	107.71	107.69
unit cell: $b$	73.77	74.95	76.61	76.83	76.99
unit cell: $c$	51.04	50.73	51.47	51.45	51.38
data resolution (Å)	1.8	2.0	3.2	2.5	2.1
$I/\sigma_1$ (av)	15.6	16.2	1.7	4.3	6.5
$I/\sigma_1$ (last shell)	6.9	10.8	1.2	2.2	2.3
completeness (%)	98.3	95.7	96.3	97.0	94.8
$R_{\text{sym}}$	0.053	0.032	0.16	0.12	0.095
refinement resolution (Å)	2.0	2.0	3.2	2.5	2.1
$R_{\text{cryst}}$	0.20	0.18	0.16	0.17	0.17
$\text{rms}_{\text{bond}}$ (Å)	0.007	0.006	0.005	0.006	0.006
$\text{rms}_{\text{angle}}$ (deg)	1.9	1.8	1.4	1.8	1.7
no. of waters	320	273	77	104	129
max est. coordinate error ( $\sigma_A$ plot) (Å)			0.281	0.169	0.157

were processed using MOSFLM (33) and SCALA (34), and reduced using the CCP4 suite of programs (34). Room-temperature data were analyzed by difference Fourier techniques using XtalView (35) and phases of existing structures prior to refinement. For frozen crystals, molecular replacement using the AMoRe package (36) was used to compensate for small differences in the unit cell observed as a result of freezing. Structure refinement used Shelxl97 (37) and repeated cycles of manual adjustment. Imidazole, phosphate, and solvent near the active site were omitted until the last cycle of refinement and were finally included with no metal distance restraints. Cavity volume calculations were performed with Voidoo (38), using a standard 1.4 Å radius probe.

## RESULTS

**Novel Phosphate-Coordinated Heme State.** A previous crystallographic study of H175G at low resolution showed that Im bound within the histidine cavity, creating an active-site similar to WT CCP without restoring peroxide-dependent oxidation of cyt *c* by the enzyme. Subsequent studies of the spectroscopic and functional properties of this mutant have now revealed unexpected properties for the Im binding kinetics, spectroscopy and reactivity that appear to be correlated with exposure to high concentrations of phosphate buffer. Crystals of H175G that were initially dissolved in 200–500 mM phosphate buffer to generate stock solutions exhibited altered kinetics for Im binding, and greatly reduced rates of reaction with peroxide relative to samples that had not been exposed to high concentrations of phosphate. This effect may impact a previous Resonance Raman study which showed that the H175G mutant, in the absence of Im, underwent a pH-dependent shift in conformation, interpreted as an equilibrium between two 5-coordinate states with water and hydroxide bound, respectively. Our more recent studies show that when phosphate buffers are avoided, the optical spectra of this mutant do not undergo the pH dependent conformational conversion noted previously (see following paper). We have thus determined the crystal structures of H175G/Im crystallized with and without high initial phosphate concentrations to characterize this effect.

Two low-temperature (100 K) structures of H175G/Im at pH 6 and containing 10 mM exogenous imidazole, are compared in Figure 1. The statistics for data collection and

refinement of these structures are given in Table 1. For one structure (H175G/Im 100 K, Figure 1A), the protein was crystallized by vapor diffusion against MPD from MES buffer, while the second structure (H175G/Im<sub>d</sub>/phosphate<sub>c</sub>, Figure 1B) was obtained by microdialysis of protein in 500 mM phosphate against 50 mM phosphate. The  $2F_o - F_c$  electron density at  $2\sigma$  of Figure 1 shows clear differences at the active site indicating the presence of a heme ligand in the distal cavity of H175G/Im<sub>d</sub>/phosphate<sub>c</sub> that is not observed for H175G/Im at 100 K. The electron density feature is well modeled by a heme-coordinated phosphate ion ( $d_{\text{Fe-O}} = 1.95$  Å) as shown in Figure 1B. In addition, imidazole is observed in the proximal histidine cavity, but the iron is domed slightly out of the heme plane toward the coordinated phosphate, resulting in a long ( $d_{\text{Fe-Im}} = 3.3$  Å) iron-imidazole vector. Thus, the heme in H175G/Im<sub>d</sub>/phosphate<sub>c</sub> appears to be in a novel 5-coordinate state containing a heme-coordinated phosphate and a dissociated proximal imidazole.

Large protein structural rearrangements are necessary to accommodate phosphate binding to H175G/Im. As indicated in Figure 1B, phosphate occupation of the distal heme cavity is incompatible with His-52 in its native conformation. The His-52 side-chain is thus repositioned in H175G/Im<sub>d</sub>/phosphate<sub>c</sub>, which in turn forces a repacking of the Asn-82 side chain that normally forms a hydrogen bond to the N<sub>δ</sub>H of His-52. These two changes in side-chain orientation result in a significant conformational rearrangement in two segments on the surface of the protein. A small, single-turn helical region between Asn-82 and Thr-70 opens to form a  $\beta$ -sheet interaction with a segment between Pro-134 and Asn-141 as shown in Figure 2. A second remarkable feature of this protein rearrangement is the way in which a group of aromatic side chains is repacked to preserve a core of hydrophobic interactions along one side of the rearranged helical segment (Figure 3). Thus, hydrophobic interactions between Y71, F77, F89, and F108 are replaced by a new core containing F73, F77, F89, and F108 in the phosphate bound structure.

**pH-Dependent Coordination of Imidazole to H175G.** Unlike WT CCP, whose coordination and functional properties are not markedly pH dependent, H175G/Im undergoes an ionization-linked dissociation of bound imidazole. Structures of H175G/Im were determined from crystals grown at

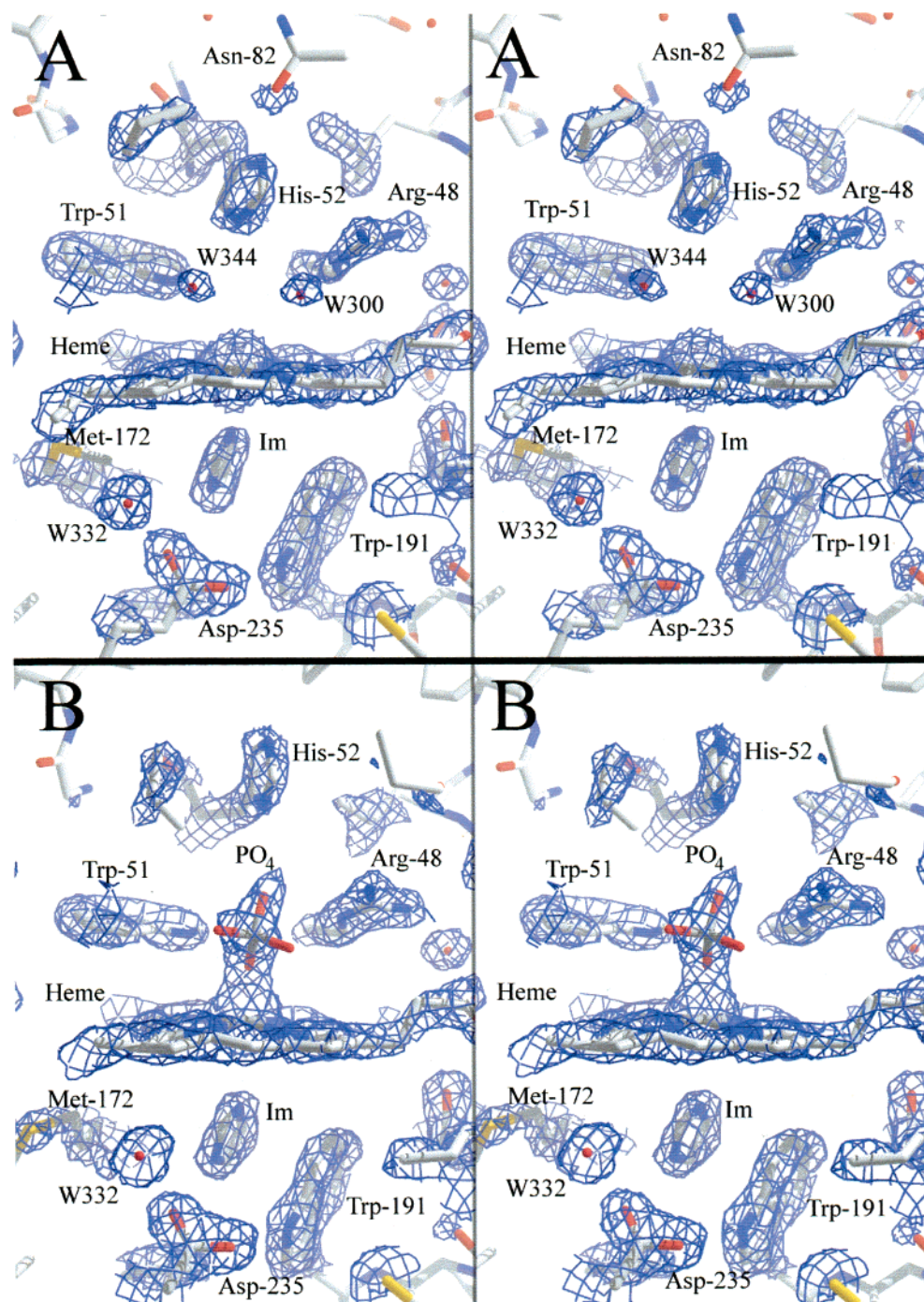


FIGURE 1: Stereoviews of the  $2F_o - F_c$  electron density for low temperature (100 K) structures of H175G/Im at pH 6, surrounding the heme active-site, in the absence (A) and presence (B) of phosphate. Phosphate-free crystals were grown by vapor diffusion against 25% MPD in MES buffer, and phosphate-containing crystals were grown by micro-dialysis from 200 mM phosphate buffer. The 100 K structure in the absence of phosphate (A) is very similar to that obtained at room temperature except that the distal water molecule is not observed at low temperature. This may be the result of MPD and/or freezing. Phosphate, however, appears to bind to the iron of the distal heme face (B), causing the dissociation of the proximal imidazole and rearrangements of the side chains of His-52 and Asn-82 in the distal cavity.

pH values of 5.2, 6.0, and 7.0. The structures were determined at room temperature to avoid potential complications from the effects of freezing and provide information attributable to pH alone. Data were collected rapidly using exposures of 2 s/frame at SSRL Beamline 7-1 to avoid problems with short crystal diffraction lifetimes at room temperature. Each data set was completed within 1 h of initial X-ray exposure on a single crystal. The  $2F_o - F_c$  electron density contoured at 1, 3, and  $5\sigma$  showing a cross-section of the heme and its axial ligands is shown in Figure 4, panels

A–C, and compared with that of WT CCP in Figure 4D. Clear changes in the coordination of both proximal Im and distal water coordination are observed as a function of pH. At pH 5, the iron is observed to be displaced out of the heme plane by  $\sim 0.3$  Å toward the distal cavity and the Im density is clearly disconnected from the iron at  $1\sigma$ . As the pH is raised to 6, the iron moves into plane and a somewhat closer interaction with the proximal Im is observed. This trend continues in the density of the structure at pH 7 (Figure 4C). Although the structure at pH 7 is most similar to that of WT

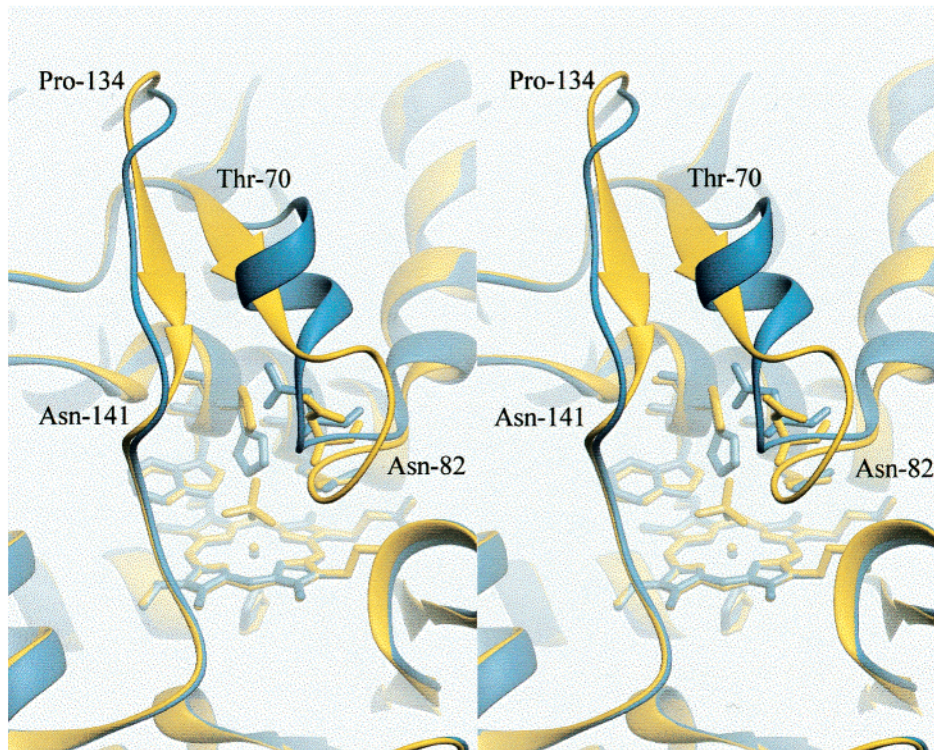


FIGURE 2: Stereoview showing a ribbon diagram of the protein conformational change resulting from phosphate coordination. Shown in blue is the structure of H175G/Im in the absence of phosphate, while that in the presence of phosphate is in yellow. A significant protein backbone rearrangement is observed between P134 and N141 and between T70 and N82 involving the conversion of a short helical turn into a  $\beta$ -sheet interaction between strands.

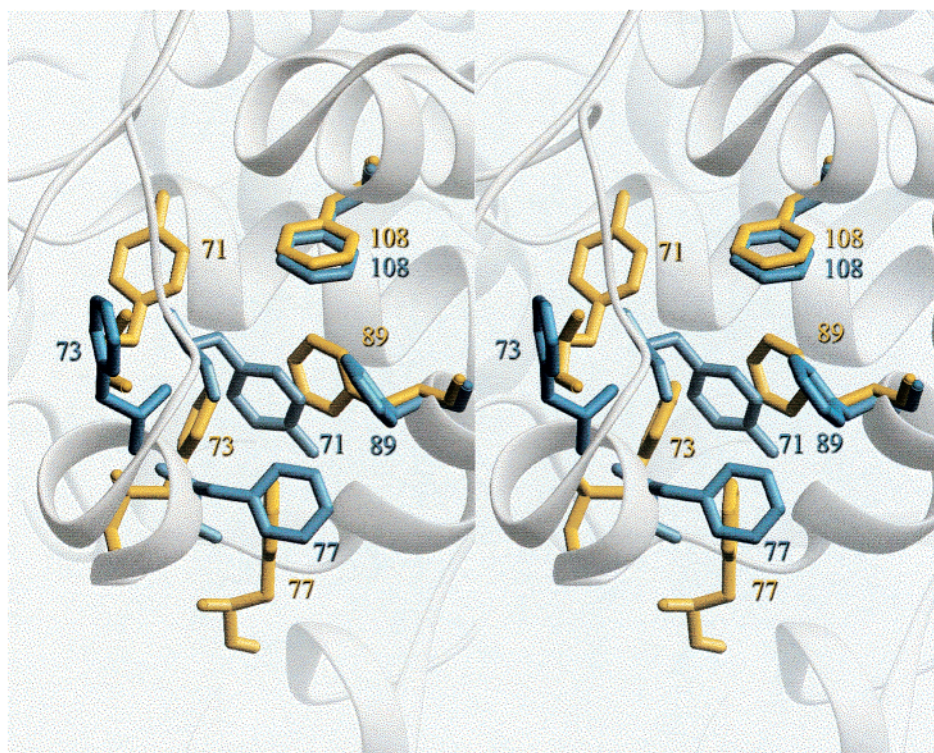


FIGURE 3: Stereoview of the repacking of a group of aromatic side chains that occurs with the conformational change associated with phosphate binding to H175G/Im. The backbone ribbon is shown for the structure in the absence of phosphate, and the side chains are colored as in Figure 2.

CCP (Figure 4D), the iron of H175G/Im pH 7 remains essentially in plane while that of WT CCP is displaced by  $\sim 0.2$  Å toward the proximal histidine.

Further analysis of the refined structures indicates that bound Im makes a tradeoff in its interactions between the

heme and Asp-235. Distances for the interactions between the iron, its ligands and Asp-235 derived from these structures are shown in Figure 5, panels A–C. At pH 5, where free imidazole is largely protonated, it is clearly dissociated from the heme ( $d_{\text{Fe-Im}} = 2.9$  Å), but is positioned

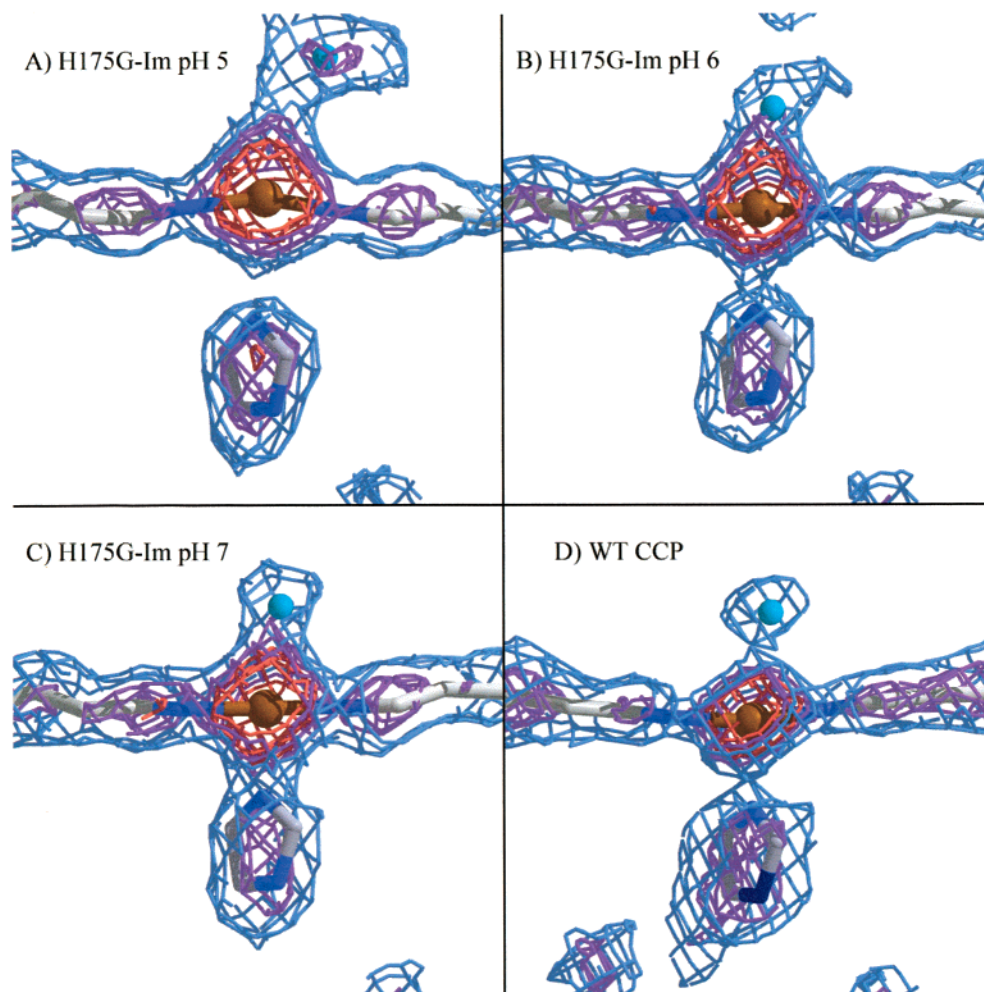


FIGURE 4:  $2F_o - F_c$  electron density maps for room-temperature structures of H175G/Im grown from solutions at pH 5 (A), pH 6 (B), and pH 7 (C) are compared with that of WT CCP (D). The contours shown are at  $+1$ ,  $3$ , and  $5\sigma$ . A thin cross-section through the heme iron is shown with the iron at the center and the heme extending horizontally.

to form an ideal hydrogen bond to Asp-235 ( $d_{\text{Asp-Im}} = 2.8$  Å). This is partially a result of the out of plane placement of the iron toward the distal cavity. The position of the distal water remains somewhat ambiguous, due to the lower resolution of this structure. The distributed electron density extending from the iron to a peak at  $3.6$  Å (Figure 4A) may represent a water molecule at this distance. However, this would result in a 4-coordinate heme state, in contrast to spectroscopic data in the following paper in this issue that show H175G/Im pH 5 is a 5-coordinate high-spin complex. Thus, as it is also possible that an additional water molecule is present at a closer distance and unresolved from the iron in this structure, we assign H175G/Im pH 5 as a 5-coordinate water bound species (H175G/Im<sub>d</sub>/H<sub>2</sub>O<sub>c</sub>).

At pH 7.0, near the  $pK_a$  of imidazole in solution, it is apparent from Figure 5C that the imidazole is coordinated to the heme with a distance ( $d_{\text{Fe-Im}} = 2.0$  Å) that is very similar to that of WT enzyme ( $d_{\text{Fe-Im}} = 2.1$  Å). However, because the iron remains close to the heme plane, the Im at this coordinating distance has moved slightly away from Asp-235 ( $d_{\text{Fe-Asp}} = 3.1$  Å), weakening the hydrogen bond to Im significantly, relative to that at lower pH or in WT CCP. The distal water is observed at a slightly shorter distance ( $d_{\text{Fe-HOH}} = 2.4$  Å) compared to WT CCP ( $d_{\text{Fe-HOH}} = 2.6$  Å), partially as a result of the in-plane iron atom. This may also account for the increased tendency of this mutant to

convert to 6-coordinate low-spin forms. Thus, at pH 7 the coordination of H175G/Im remains 5-coordinate with the proximal imidazole coordinated to the iron and a dissociated distal water (H175G/Im<sub>c</sub>/H<sub>2</sub>O<sub>d</sub>) as is observed in WT CCP.

Distances obtained from the structure determined at pH 6 (Figure 5B) are intermediate between those at pH 5 and 7 in every aspect. This independent observation provides strong support for the structural changes noted above. Although the intermediate distances observed at pH 6 might represent an intermediate conformational state, they more likely result from an average of two conformational extremes. Indeed, it was found possible to refine this structure using partial occupancies of the pH 5.2 and 7.0 structures: 48 and 52%, respectively.

**Effects of Temperature.** The only significant difference observed between the structure of H175G/Im pH 6 determined at room temperature (Figure 5B) and H175G/Im at 100 K (Figure 1A) concern distal cavity water occupation. While each of the structures at room temperature show clear evidence for the distal water molecule above the heme plane at  $2.3$ – $2.6$  Å from the iron, no evidence for this water molecule was seen in the low temperature structure of Figure 1A. Instead, two additional ordered water molecules, HOH-300 and HOH-344, are observed in the opening to the peroxide access channel that are not evident at room temperature. Such additional ordered solvent is expected at

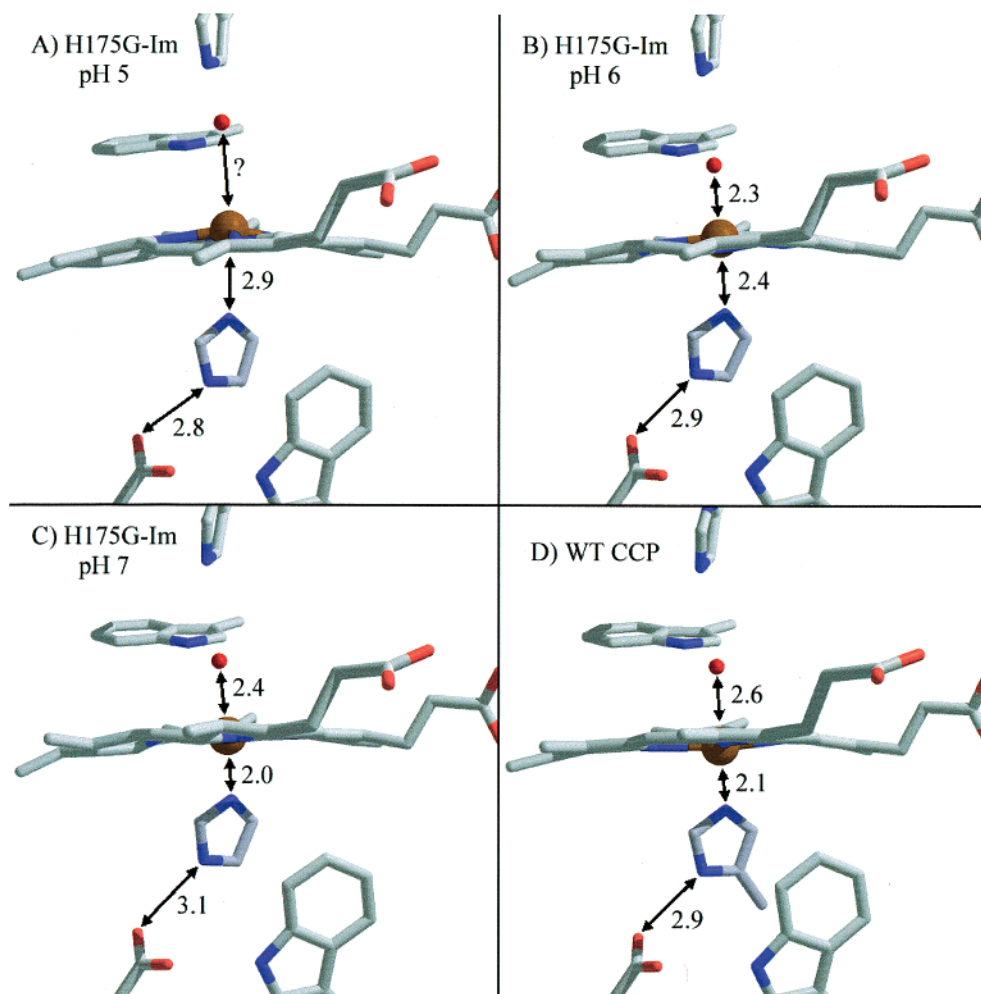


FIGURE 5: Refined models corresponding to the electron density of Figure 4 are shown with the metal ligand and Asp235 hydrogen bonding distances derived from the refinements. At pH 7, the coordination state, H175G/Im<sub>d</sub>/H<sub>2</sub>O<sub>d</sub>, is similar to that of WT CCP, but has a somewhat weaker hydrogen bond to Asp-235. As the pH is lowered to 5, Im dissociates from the heme and forms a stronger hydrogen bond to Asp-235. Distal coordination by water at pH 5 is uncertain due to the distributed electron density, but spectroscopic data (see the following paper in this issue) indicates coordination is represented by H175G/Im<sub>d</sub>/H<sub>2</sub>O<sub>d</sub>.

low temperature; indeed approximately 300 waters were fit into the density of the low-temperature structures, while only one-third this number were observed in the room temperature structures (Table 1). The absence of the distal water at low temperature is thus striking and unexpected, and may result from the combined subtle effects of heme iron movements, and/or changes in the effective activity coefficient of water due to MPD used as cryosolvent. Nevertheless, the structures of H175G/Im at pH 6 are otherwise essentially identical at the two temperatures and provide a basis for the comparison of functional and spectroscopic properties of the following paper in this issue.

Finally, an additional change in the protein backbone near the H175G mutation site is observed in each of the H175G structures reported here that was not fully characterized in the earlier room-temperature structure of H175G (21). The protein backbone between residues A174 and A176 is observed in an alternate conformation in H175G with respect to WT CCP (not shown). This alternate conformation is possible with only minor shifts in the surrounding structure due to the small side chain volumes in the sequence between residues 174 and 176.

## DISCUSSION

A number of conclusions can be made from this study about the role played by the axial ligand in heme enzymes. The results directly address such issues as the sensitivity of heme reactivity to axial ligand identity, the control of heme coordination and distortion by intrinsic vs steric factors, and conformational changes induced by ligand binding.

Steric and noncovalent interactions with the protein in the distal and proximal heme cavities dictate which face is coordinated by a given exogenous ligand, yet conformational changes are possible which allow unanticipated changes in this ligand binding specificity. In the H175G mutant, a cavity exists on both sides of the heme, and it is not immediately clear which side will be utilized by coordinating ligands. Im binds within the proximal cavity, presumably due to the ideal steric template formed by deletion of the His-175 side chain, and because hydrogen-bonding interactions with Asp-235 can be approximately restored. However, coordination of phosphate was unexpected because it is too large to occupy either the proximal or distal cavity. In this case, an alternate conformation is energetically accessible that is compatible with phosphate occupation of the distal cavity. It is interesting

that this phosphate effect is not observed with the WT enzyme. This indicates either that additional energy is stored in the iron–histidine bond of WT CCP relative to the iron–Im bond of H175G/Im, or that the tethered His-175 is sterically more rigid, preventing proximal imidazole dissociation that accompanies distal phosphate coordination.

Several subtle features in the structures of H175G/Im indicate that Im is a weaker heme ligand than the native His-175. First, the dependence of iron out-of-plane displacement on axial ligand environment is reflected in the structures of H175G/Im as a function of pH. High-spin ferric hemes with asymmetric 5- and 6-coordination generally show iron displacements of  $\sim 0.4$  Å from the heme plane toward the strongest axial ligand, because the occupied  $d_{x^2-y^2}$  orbital is too large to fit fully within the porphyrin core (4). Consistent with this, the iron in WT CCP is displaced  $\sim 0.2$  Å toward the proximal His-175 ligand (28). However, the structure of H175G/Im pH 7 shows that Im is coordinated to the iron, but the electron density for the iron is essentially in the heme plane. This observation may reflect actual absence of an out-of-plane distortion, but it may also result from an average of conformations in which the iron is displaced above and below the heme plane. However, the refined *B* factor for the iron of H175G/Im pH 7 ( $12.3$  Å<sup>2</sup>) is essentially identical to that of WT CCP ( $12.5$  Å<sup>2</sup>), indicating that disorder is not responsible for the apparent in-plane iron. Studies of model complexes have shown that symmetric 6-coordinate high-spin hemes can remain in-plane by porphyrin core size expansion (39). Thus, the coordinated Im of the pH 7 structure appears to behave as a somewhat weaker ligand than the native histidine as reflected by the more planar heme. For H175G/Im pH 5, where the imidazole in the proximal cavity has dissociated from the iron, the iron displacement shifts to the distal side. This suggests that the distal face now contributes the strongest axial ligand, and while the resolution of the pH 5 structure is not sufficient for its direct observation, these data suggest distal water coordination. In support of this assignment, spectroscopic data (in the following paper in this issue) clearly indicate that this state is 5-coordinate. The simplest interpretation for Im dissociation involves its protonation with a  $pK_a$  near 6, forcing the heme to relinquish its ligand for a weaker 5-coordinate aquo form. This suggests that the  $pK_a$  for Im within the H175G cavity is similar to that in solution. A similar transition is not observed for WT CCP, and this indicates that steric tethering of His-175 near the heme may play a role in reducing its effective  $pK_a$  relative to Im.

The conclusions of this study have helped to define the subtle structural differences that prevent an untethered Im from serving as an accurate functional replacement for the axial histidine ligand in CCP. The evidence that Im forms a significantly weaker interaction with the iron than the native histidine indicates a role for the protein tether in maintaining the strength of this interaction. While in the cavity, the Im undergoes a pH-dependent ionization allowing neutral and imidazolium states to be populated. At pH 5, it is dissociated from the heme yet makes a strong hydrogen bond to Asp-235. As a result, the iron is displaced from the heme plane toward the distal side, where it may be coordinated to a water molecule. In this state, the protein is functionally impaired with respect to its reaction with peroxide (see following paper in this issue). As the pH is increased first to 6 and then 7, a

systematic change is noted in the active-site structure in which the iron moves toward the proximal heme face, Im moves toward the heme to a coordinating distance of  $2.0$  Å, and the distal water moves away from the heme to a position near that of WT CCP. Thus the heme remains 5-coordinate, but is now bound to the proximal Im. However, the iron does not appear to be displaced as far out-of-plane toward the proximal side as in WT, so the additional movement required for the Im to coordinate the heme comes at the expense of a weaker hydrogen bond to Asp-235. This situation is somewhat different from the H93G mutant of Mb (20), where the heme is also less domed in the Im complex compared to the WT enzyme. In the case of H93G Mb, the Im rotates significantly about the Im–Fe axis to improve hydrogen bonding with a nearby serine, and it was proposed that this rotation away from an orientation in which the Im eclipses opposite heme pyrrole nitrogens allows closer approach of the Im to the heme. In CCP, His-175 also eclipses opposite heme pyrrole nitrogens. However, Asp-235 is prepositioned for hydrogen bonding, and therefore no rotation of the Im is observed. Finally, while the heme coordination of the H175G/Im complex at pH 6–7 is much like that of the WT enzyme, under no condition has the Fe–Asp–His linkage been precisely restored. The spectroscopic and functional consequences of this subtle variation are explored in the following paper in this issue.

#### ACKNOWLEDGMENT

The authors would also like to thank Drs. Gerard Jensen, Rabi Musah, Melissa Fitzgerald, Alycen Pond, and Mark Roach for help and valuable discussions. This work is based upon research conducted at the Stanford Synchrotron Radiation Laboratory (SSRL), which is funded by the Department of Energy (BES, BER) and the National Institutes of Health (NCRR, NIGMS).

#### REFERENCES

1. Bruice, T. C. (1986) *Ann. N. Y. Acad. Sci.* **471**, 83–98.
2. Groves, J. T., and Viski, P. (1989) *J. Am. Chem. Soc.* **111**, 8537–8538.
3. Scheidt, W. R., and Ellison, M. K. (1999) *Acc. Chem. Res.* **32**, 350–359.
4. Scheidt, W. R., and Gouterman, M. (1983) *Iron Porphyrins*, Part 1, Addison-Wesley, Reading, MA.
5. Traylor, T. G. (1981) *Acc. Chem. Res.* **14**, 102–109.
6. Traylor, T. G., Lee, W. A., and Stynes, D. V. (1984) *J. Am. Chem. Soc.* **106**, 755–764.
7. Gajhede, M., Schuller, D. J., Henriksen, A., Smith, A. T., and Poulos, T. L. (1997) *Nat. Struct. Biol.* **4**, 1032–1038.
8. Poulos, T. L. (1993) *Curr. Opin. Biotechnol.* **4**, 484–489.
9. Poulos, T. L. (1995) *Curr. Opin. Struct. Biol.* **5**, 767–774.
10. Choudhury, K., Sundaramoorthy, M., Hickman, A., Yonetani, T., Woehl, E., Dunn, M. F., and Poulos, T. L. (1994) *J. Biol. Chem.* **269**, 20239–20249.
11. Matsui, T., Nagano, S., Ishimori, K., Watanabe, Y., and Morishima, I. (1996) *Biochemistry* **35**, 13118–13124.
12. Goodin, D. B. (1996) *J. Biol. Inorg. Chem.* **1**, 360–363.
13. Poulos, T. L. (1996) *J. Biol. Inorg. Chem.* **1**, 356–359.
14. Ellman, J. A., Mendel, D., and Schultz, P. G. (1992) *Science* **255**, 197–200.
15. Toney, M. D., and Kirsch, J. F. (1989) *Science* **243**, 1485–1488.
16. Eriksson, A. E., Baase, W. A., Wozniak, J. A., and Matthews, B. W. (1992) *Nature* **355**, 371–373.
17. Denblauwen, T., Vandekamp, M., and Canters, G. W. (1991) *J. Am. Chem. Soc.* **113**, 5050–5052.

18. Denblauwen, T., and Canters, G. W. (1993) *J. Am. Chem. Soc.* 115, 1121–1129.
19. Fitzgerald, M. M., Churchill, M. J., McRee, D. E., and Goodin, D. B. (1994) *Biochemistry* 33, 3807–3818.
20. Barrick, D. (1994) *Biochemistry* 33, 6546–6554.
21. McRee, D. E., Jensen, G. M., Fitzgerald, M. M., Siegel, H. A., and Goodin, D. B. (1994) *Proc. Natl. Acad. Sci. U.S.A.* 91, 12847–12851.
22. Wilks, A., Sun, J., Loehr, T. M., and Ortiz de Montellano, P. R. (1995) *J. Am. Chem. Soc.* 117, 2925–2926.
23. Decatur, S. M., Franzen, S., DePillis, G. D., Dyer, R. B., Woodruff, W. H., and Boxer, S. G. (1996) *Biochemistry* 35, 4939–4944.
24. Musah, R. A., and Goodin, D. B. (1997) *Biochemistry* 36, 11665–11674.
25. Edwards, S. L., Xuong, N. H., Hamlin, R. C., and Kraut, J. (1987) *Biochemistry* 26, 1503–1511.
26. Choudhury, K., Sundaramoorthy, M., Mauro, J. M., and Poulos, T. L. (1992) *J. Biol. Chem.* 267, 25656–25659.
27. Smulevich, G., Neri, F., Willemsen, O., Choudhury, K., Marzocchi, M. P., and Poulos, T. L. (1995) *Biochemistry* 34, 13485–13490.
28. Finzel, B. C., Poulos, T. L., and Kraut, J. (1984) *J. Biol. Chem.* 259, 13027–13036.
29. Goodin, D. B., and McRee, D. E. (1993) *Biochemistry* 32, 3313–3324.
30. Miller, M. A., Vitello, L., and Erman, J. E. (1995) *Biochemistry* 34, 12048–12058.
31. Millett, F., Miller, M. A., Geren, L., and Durham, B. (1995) *J. Bioenerg. Biomembr.* 27, 341–351.
32. Pelletier, H., and Kraut, J. (1992) *Science* 258, 1748–1755.
33. Leslie, A. G. W. (1999) *Acta Crystallogr., Sect. D* 55, 1696–1702.
34. Bailey, S. (1994) *Acta Crystallogr., Sect. D* 50, 760–763.
35. McRee, D. E. (1999) *J. Struct. Biol.* 125, 156–165.
36. Navaza, J. (1994) *Acta Crystallogr.* 50, 157–163.
37. Sheldrick, G. M., and Schneider, T. R. (1997) *Methods Enzymol.* 277, 319–343.
38. Kleywegt, G. J., and Jones, T. A. (1994) *Acta Crystallogr., Sect. D* 50, 178–185.
39. Scheidt, W. R., Cohen, I. A., and Kastner, M. E. (1979) *Biochemistry* 18, 3546–3551.

BI002089R